Chemical Engineering Journal 144 (2008) 518–530

Contents lists available at ScienceDirect

Chemical Engineering Journal

journal homepage: www.elsevier.com/locate/cej

Growth of nitrogen-doped filamentous and spherical carbon over unsupported and Y zeolite supported nickel and cobalt catalysts

Antonio Nieto-Márquez[a,*], José C. Lazo[b], Amaya Romero[a], José L. Valverde[a]

[a] Facultad de Ciencias Químicas, Departamento de Ingeniería Química, Universidad de Castilla-La Mancha, Campus Universitario s/n, 13071 Ciudad Real, Spain
[b] Sección Química, Departamento de Ciencias, Pontificia Universidad Católica del Perú, Av. Universitaria 1801, Lima 32, Peru

ARTICLE INFO

Article history:
Received 14 April 2008
Received in revised form 24 July 2008
Accepted 29 July 2008

Keywords:
Acetonitrile decomposition
Y zeolite
Carbon nanofilaments
Carbon nanospheres

ABSTRACT

Unsupported and Y zeolite supported nickel and cobalt catalysts have been tested for the growth of nitrogen-doped structured carbon via the chemical vapour decomposition (CVD) of acetonitrile where 550 °C ≤ T ≤ 1150 °C. A range of carbonaceous structures, including carbon filaments with different lattice structures and carbon nanospheres were obtained. The graphitic character of the carbon product has been evaluated by means of temperature-programmed oxidation (TPO) and XRD analyses, surface area and porosity measurements for both catalyst and carbon product are provided and structural/morphological features illustrated by scanning and transmission electron microscopy (SEM and TEM). Carbon yield and morphology were strongly dependent on reaction temperature, the nature of the active metal and the use of a support. Carbon yield increased with increasing temperature (up to 1050 °C) to give maximum values in the order Ni < Co < Ni/Y < Co/Y. The supported catalysts delivered significantly higher carbon yields (up to 35 g_{carbon}/g_{metal}) and initiated carbon growth at temperatures up to 300 °C lower than that observed for the bulk metals. Carbon generated over Ni/Y and Co/Y at 750 °C took the form of high aspect ratio nanofibres where the arrangement of graphene layers exhibited a periodic variation at higher reaction temperatures to ultimately result in a predominant production of nanospheres at 1150 °C, rather attributed to a thermal than a catalytic route. Based on TPO analyses, carbon grown from bulk and supported Ni showed a higher degree of structural order compared with the Co promoted growth. An increase in reaction temperature served to enhance graphitic character. XRD analyses were in all the cases consistent with a graphitic product. Elemental (CHN) analysis of the carbon product has revealed a nitrogen content of up to 5 mol%.

1. Introduction

The discovery of structured carbonaceous materials, notably carbon nanotubes and nanofibres [1], with a diversity of unique physical and chemical properties has attracted a significant research effort largely focused on controlled synthesis and developing new applications in gas adsorption [2], H_2 storage [3] and electronics [4]. In addition, structured carbon has been used as catalyst support [5] and as an electrochemical promoter in fuel cells [6]. Doping these carbonaceous structures with heteroatoms, such as nitrogen or boron, is an effective means of modifying surface and electronic properties [7,8]. Indeed, it has been established that the incorporation of nitrogen in nanotubes results in enhanced conductivity, polarity and basicity, while modifying surface hydrophilicity [9].

Arc discharge and laser ablation have been employed in the synthesis of structured carbon [10,11] but these methods also produce a significant quantity of undesired by-products, such as carbon soot, that necessitates additional purification steps. Moreover, the associated low yields and high energy requirements have served as the impetus for the development of more efficient carbon production processes. A catalytic route, often termed chemical vapour decomposition (CVD), has emerged as a lower cost option which exhibits a greater degree of control and a more feasible scale-up [12]. CVD synthesis is now established using transition metals, such as Fe, Co and Ni [13]. Baker and co-workers [14] and Toebes et al. [15] have reported carbon growth over supported and unsupported metals where catalyst performance depended on the nature of the metal, the support and the reactivity of the carbon-containing gas. The interaction of the metal with a support can play a critical role in determining both carbon structure and yield. There have been a number of published CVD studies [16,17] that employed metals supported on amorphous oxides, e.g., silica and alumina. Hernadi and co-workers [18] recorded the first application of microporous crystalline zeolites (Y and ZSM-5) as support material where they

* Corresponding author. Tel.: +34 926295300; fax: +34 926295256.
E-mail address: antonio.nieto@uclm.es (A. Nieto-Márquez).

1385-8947/$ – see front matter © 2008 Elsevier B.V. All rights reserved.
doi:10.1016/j.cej.2008.07.046

Table 1
Metal content, BET surface area, porosity and surface acidity associated with the catalysts considered in this study

Sample	BET surface area (m^2/g)	Ext. surface area (m^2/g)[a]	Micropore volume (cm^3/g)	Meso- and Macro-pore volume (cm^3/g)	Acidity (mmol NH_3/g)	Metal content (%, w/w)
Parent Y zeolite	828	3 (<1%)	0.312	0.008	0.214	–
Ni/Y	512	42 (8%)	0.183	0.137	1.351	20
Co/Y	471	94 (20%)	0.145	0.175	1.088	20
Ni + Y[b]	3	3	–	–	–	20
Co + Y[b]	2	2	–	–	–	20

[a] Values in parenthesis represent the external surface area as a percentage with respect to the total.
[b] Values refer to the bulk metal.

noted certain advantages over silica, notably a more facile purification as zeolites dissolve more readily than silica in strong acids. The general consensus [12,15,16] to emerge is that the use of supported catalysts facilitates the formation of narrower carbon fibres/tubes. Yu and co-workers have, however, noted [19] that this is not universally true in that unsupported Fe can also promote the growth of uniformly narrow carbon tubes when employing less reactive carbon precursors.

Compounds which have served as reactants in CVD syntheses include CO [20], methane [21], acetylene [20] and ethylene [13] with decomposition temperatures in the range 400–700 °C. With a view to generating a nitrogen-containing carbonaceous product, such carbon precursors as pyridine [22], dimethylformamide [23], aniline [24] and acetonitrile [25] have been considered where nitrogen can be considered an "n-type" dopant with an extra electron for donation when replacing carbon in the graphitic matrix. As nitrogen-containing hydrocarbons are less reactive, reaction temperatures in the range 800–1000 °C are required [22–25]. In earlier work, we reported the growth of structured carbon via the decomposition of ethylene over Y zeolite supported Ni [26,27] and recorded reproducible yields of uniformly sized carbon nanofibres. This work has since been extended to consider carbon growth over bulk and Y zeolite supported Ni and Co, using acetonitrile as the carbon precursor. In this work, the effect of temperature, reaction time, the nature of the active metal and the role of zeolite as support on carbon yield are considered while carbon structural features (morphology, aspect ratio and graphitic nature) are characterised. In the present work we report an unexpected shift in the predominant carbon growth from filament to nanosphere formation, were thermal decomposition is proposed to control the growth of the latest rather than catalysis. The viability of incorporating nitrogen in the carbon product is also addressed.

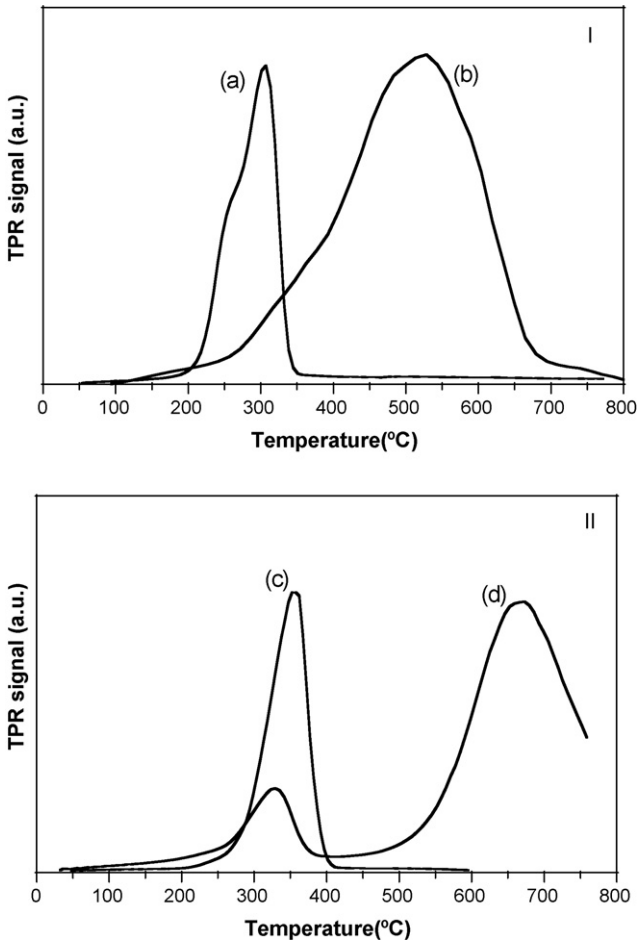

Fig. 1. TPR profiles generated for the reduction of I (a) Ni + Y, (b) Ni/Y and II (c) Co + Y and (d) Co/Y.

2. Experimental

2.1. Catalyst preparation

20% (w/w) Y zeolite (Zeolyst International) supported Ni and Co samples were prepared by homogeneous deposition–precipitation, as described in detail by Toebes et al. [15]. The as prepared catalyst precursors were filtered, thoroughly washed with deionised water and dried at 120 °C overnight. After drying, the catalysts were calcined in static air at 600 °C using a 10 °C min^{-1} ramp and maintained at that temperature for 4 h. Before use, the catalyst precursors were sieved into a batch of 249 μm average particle diameter. Carbon growth was examined over Y zeolite supported and unsupported Co and Ni. In the latter case, commercial NiO (Aldrich) and Co_3O_4 (Panreac) served as catalyst precursor in a physical mixture with the zeolite to achieve a 20% (w/w) metal content.

2.2. Catalytic synthesis of carbon nanostructures

Carbon growth was carried out at atmospheric pressure over the temperature range 550–1150 °C in a continuous flow fixed bed catalytic reactor (quartz tube, 3 cm i.d. × 60 cm) mounted in a temperature programmable oven. In each synthesis run, 200 mg of the catalyst precursor was reduced/activated by heating (10 °C min^{-1}) in 100 cm^3 min^{-1} dry 20% (v/v) H_2/He to 600 °C, which was held for 1 h. The activated catalyst was thoroughly flushed in dry He for 1 h and subsequently brought to the ultimate reaction temperature before introducing the acetonitrile/He feed (GHSV = 16,000 h^{-1}, 0.73 g_C $g_{metal}{}^{-1}$ min^{-1}). Carbon growth was monitored for up to 2 h on-stream: a reaction time of 1 h was taken as standard. The reactor was cooled to room temperature in a flow of He prior to off-line analyses. The specific carbon yields (Y_{carbon}) reported in this paper represent the gravimetric ratio of solid carbon product to the metal

content in the catalytic bed (g_c/g_{metal}), where Y_{carbon} values from repeated runs were reproducible to better than ±10%. The catalyst was removed from the carbon product by contacting with HF (48%) overnight under vigorous stirring, followed by filtration and washing.

2.3. Catalyst/carbon characterization

Powder X-ray diffractograms (XRD) were recorded with a Philips PW 1710 instrument using Ni-filtered Cu Kα radiation. Surface area/porosity measurements were conducted using a Micromeritics ASAP 2010 sorptometer apparatus with N_2 as sorbate at 77 K. Samples were outgased (at 6.6×10^{-9} bar) at 180 °C overnight prior to analysis. Specific total pore volumes were evaluated from N_2 uptake at a relative pressure (P/P_0) = 0.99. The Horvath–Kawazoe method was used to determine microporous surface area and micropore volume; mesoporosity was evaluated using the standard BJH treatment. Catalyst metal loading was determined (to better than within ±1%) by atomic absorption (AA) spectrophotometry, using a SPECTRA 220FS analyzer. Surface acid site concentration was measured by temperature-programmed desorption of ammonia (TPD_{NH_3}) using a Micromeritics TPD/TPR 2900 analyzer. The catalyst was reduced/activated under the conditions used prior to catalysis, cooled to 180 °C and the sample contacted with a flow of NH_3 for 15 min with a subsequent purge with He for 1 h to remove physisorbed NH_3. The sample was ramped at 15 °C min^{-1} from 180 to 600 °C and TPD_{NH_3} data acquired; surface acidity was related to NH_3 release as discussed in detail elsewhere [26,27]. The temperature-programmed reduction (TPR) profiles were determined using the same Micromeritics unit as for TPD analyses, where the catalyst precursor was first outgassed and heated in an Ar/H_2 flow (≥99.999% purity, 83/17 volumetric ratio) at 10 °C min^{-1} to 800 °C; the effluent gas was directed through a liquid N_2 trap and H_2 consumption was determined by TCD. Metal and carbon morphology/dimensions were analyzed by transmission (JEOL JEM-4000EX, accelerating voltage of 400 kV) and scanning (JEOL JSM-6535F) electron microscopy. Suitable specimens for TEM analyses were prepared by ultrasonic dispersion in acetone with a drop of the resultant suspension evaporated onto a holey carbon supported grid. Samples for SEM analyses were deposited on a standard aluminium SEM holder and coated with gold. Metal particle size distributions presented in this report are based on particle counts in excess of 400. Temperature-programmed oxidation (TPO) profiles of the acid treated carbon product were obtained using a PerkinElmer TGA7 thermogravimetric analyzer where a 10-mg demineralised sample was ramped from room temperature to 1000 °C at 5 °C min^{-1} in a 50 cm^3 min^{-1} O_2/He (5%, v/v). The carbon, hydrogen and nitrogen (CHN) content in the solid carbon deposits was determined using a LECO CHNS-932 apparatus. The carbon (ca. 2 mg) combustion (at 950 °C) products were analysed by IR (for C and H content) and TCD (for N content).

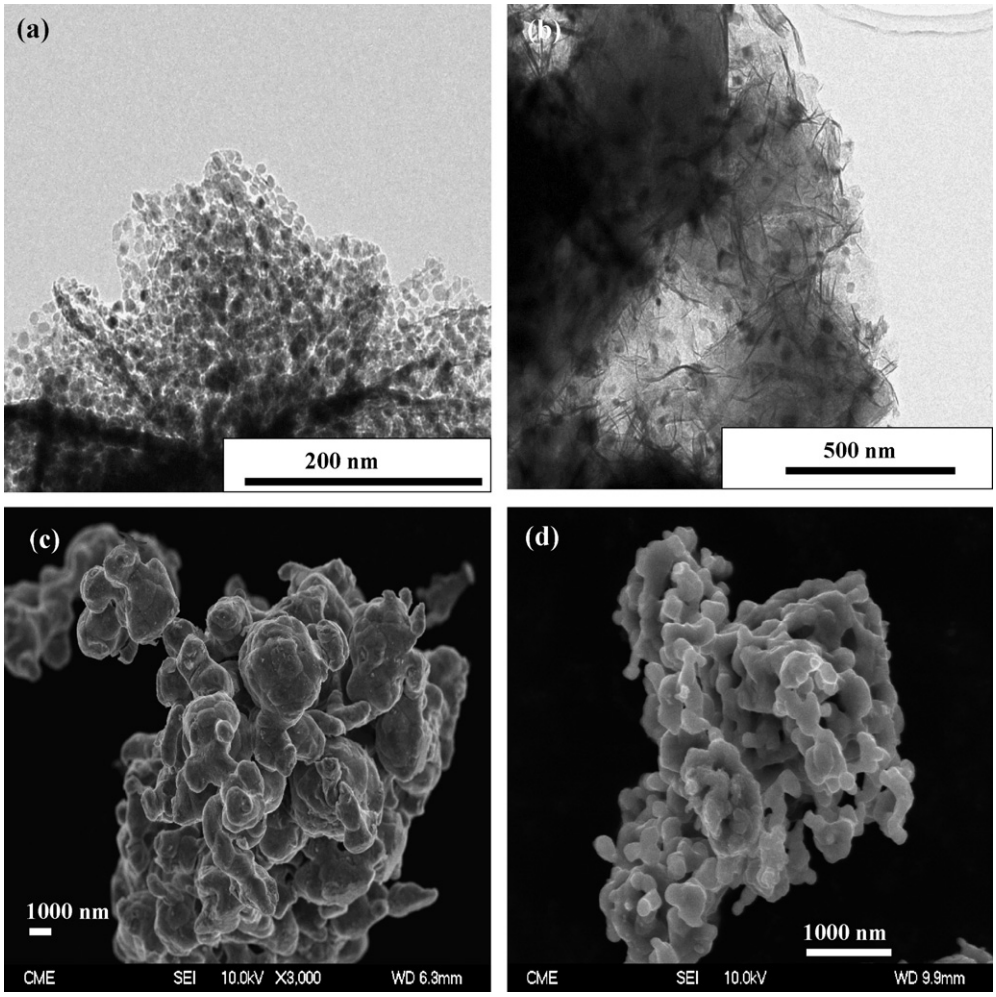

Fig. 2. Representative TEM micrographs of activated Y zeolite supported (a) Ni and (b) Co and SEM micrographs of activated unsupported (c) Ni and (d) Co.

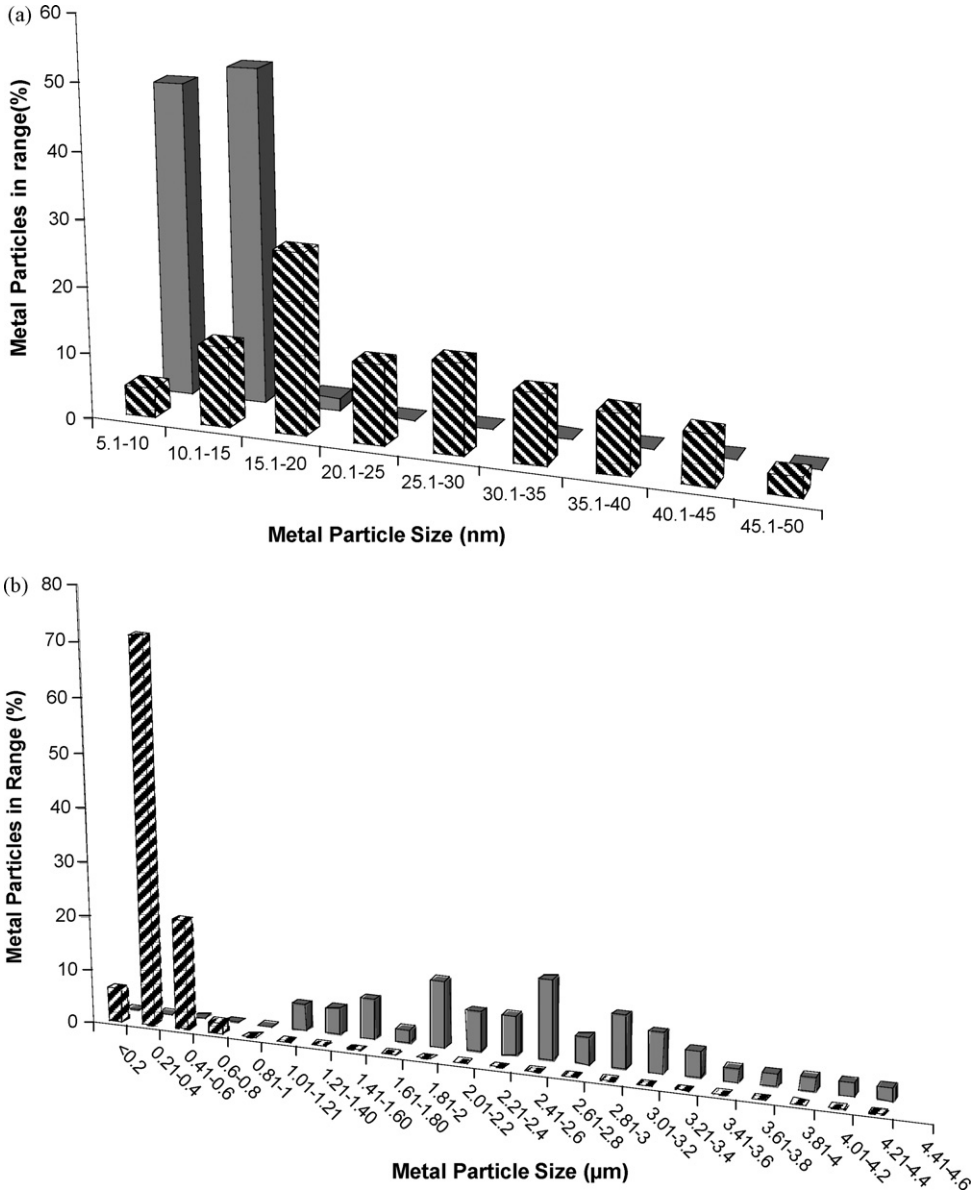

Fig. 3. Metal particle size distributions for the activated (a) Y zeolite supported and (b) unsupported Ni (solid bars) and Co (hatched bars) catalysts.

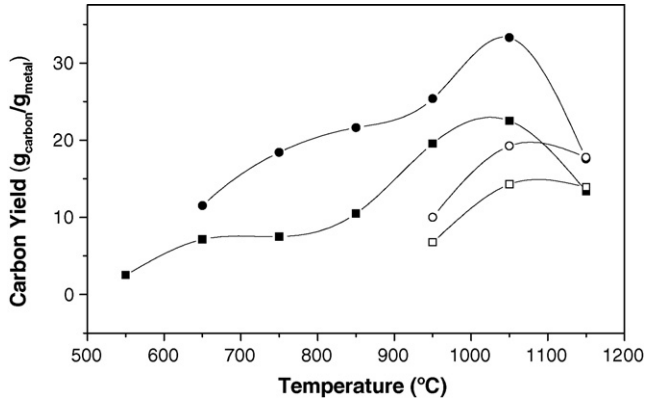

Fig. 4. Carbon yield as a function of reaction temperature over (■) Ni/Y, (●) Co/Y, (□) Ni + Y and (○) Co + Y: GHSV = 16,000 h^{-1}; 0.73 g_C g_{metal}^{-1} min^{-1}; Δt = 60 min.

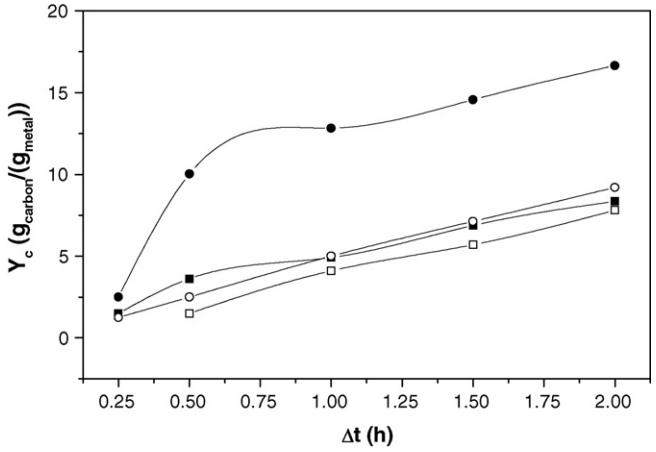

Fig. 5. Carbon yield as a function of time-on-stream over (■) Ni/Y, (●) Co/Y, (□) Ni + Y and (○) Co + Y: GHSV = 16,000 h^{-1}; 0.73 g_C g_{metal}^{-1} min^{-1}; T = 750 °C for Ni/Y and Co/Y; T = 950 °C for Ni + Y and Co + Y.

3. Results and discussion

3.1. Catalyst characterization

Critical structural characteristics of the catalysts considered in this study are given in Table 1. The introduction of either metal (Ni or Co) was accompanied by a decrease in surface area relative to the starting zeolite, which can be attributed to a partial blockage of the zeolite pores. While the external surface area of the parent Y zeolite was negligible when compared with the total area, the contribution of external area to the overall value was greater for the metal loaded samples. The decrease in BET area was accompanied by a significant drop in micropore value, a response that was more marked in the case of Co/Y. The bulk metals were characterized by low specific surface areas and limited porosity. The TPR profiles generated for the bulk and zeolite supported Ni and Co samples are presented in Fig. 1. The reduction of the bulk metal oxides generated a single H_2 consumption peak with an associated T_{max} at 305 and 355 °C for Ni and Co, respectively. Murthy et al. [28] attributed a peak at 270 °C to the direct reduction of bulk NiO while Arnoldy and Moulijn [29] ascribed a peak at T_{max} = 317 °C to a two-step reduction of Co_3O_4 to Co via CoO. The supported catalysts required higher reduction temperatures which can be attributed to metal-support interactions, an effect that is now well established [16] for supported metal systems. TPR of the supported Ni catalyst generated a broad reduction peak (T_{max} = 520 °C) with a low temperature shoulder (T_{max} = 365 °C). The latter peak arises at a higher temperature than that recorded for unsupported NiO and that can be attributed to the reduction of a precipitated hydroxide species that interacts weakly with the support. Significantly

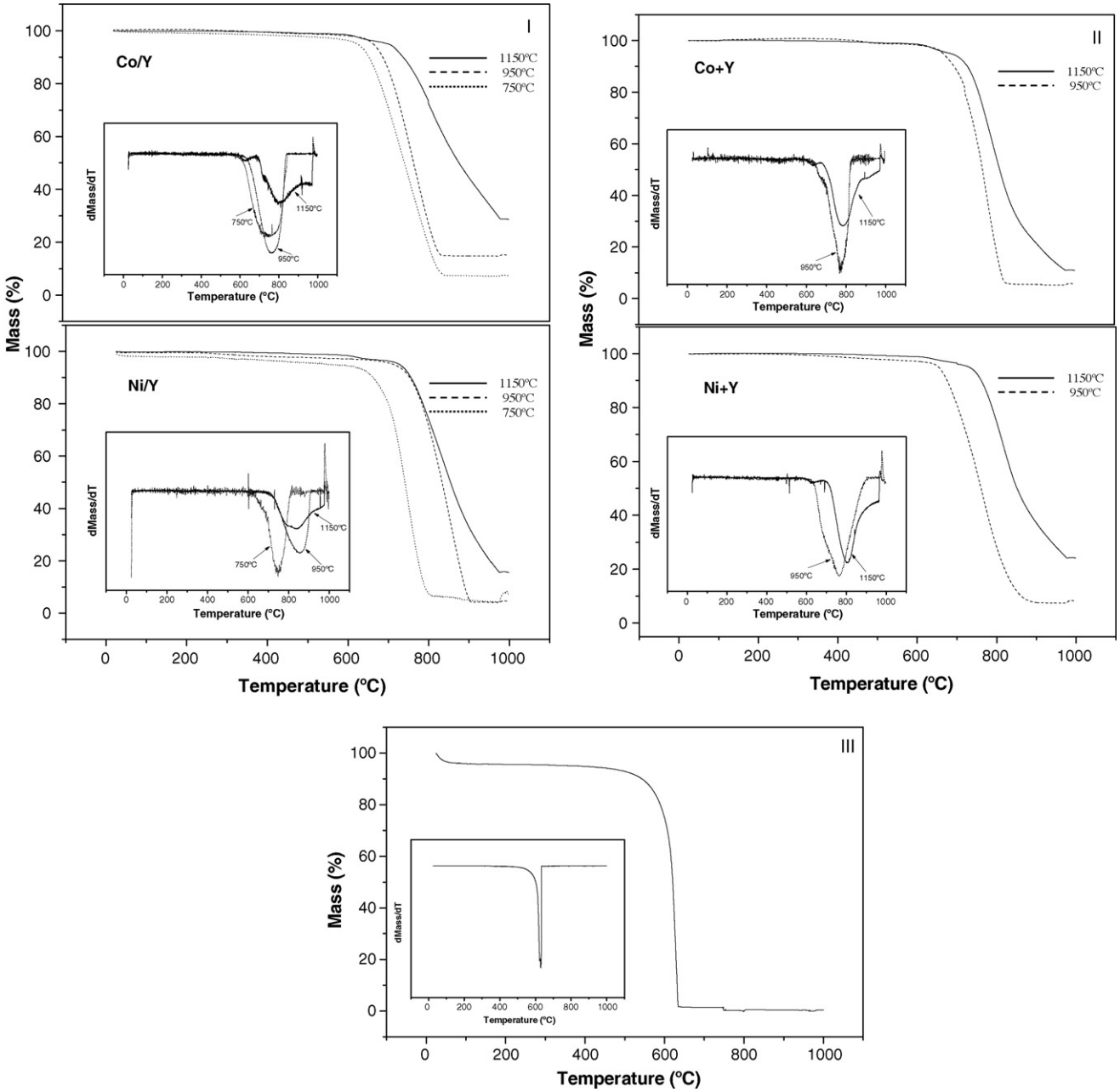

Fig. 6. TPO profiles associated with the carbon obtained at 750 °C (dotted line), 950 °C (dashed line) and 1150 °C (solid line) for reaction over (I) Y zeolite supported and (II) unsupported Ni and Co catalysts: GHSV = 16000 h^{-1}; 0.73 g_C g_{metal}^{-1} min^{-1}; Δt = 60 min. (III) TPO profile for model-activated carbon. Insets: DTG profiles.

Table 2
Range of gasification temperatures associated with carbon generated over the four catalyst systems at representative reaction temperatures: Δt = 60 min; 0.73 g_C g_{metal}^{-1} min^{-1}; carbon obtained in the absence of catalyst and model-activated (amorphous) carbon are included as reference

Catalyst	Reaction temperature (°C)	Gasification temperature range (°C)
Ni/Y	750	626–816
	950	703–903
	1150	703–>1000
Ni + Y	950	620–905
	1150	684–>1000
Co/Y	750	577–850
	950	618–840
	1150	682–>1000
Co + Y	950	609–840
	1150	670–>1000
None	1150	680–>1000
Activated carbon		500–630

greater hydrogen consumption occurs at a higher temperature and must result from the reduction of 1:1 nickel phylosilicate which has been shown to form on Ni/zeolite systems prepared by precipitation/deposition [30]. The profile generated for Co/Y is characterized by a low temperature peak with a T_{max} = 350 °C that roughly corresponded to the reduction of bulk Co_3O_4 and a higher temperature (T_{max} = 670 °C) H_2 consumption that can be linked to the reduction of Co species that interact strongly with the support. It should be noted that the TPR profile for Co/Y ultimately returned to baseline during the final isothermal hold. Surface acidity was increased (see Table 1) with the incorporation of the metal due to of the introduction of surface OH groups during catalyst preparation as has been noted elsewhere [31]. Metal particle size and morphology in the samples post-TPR were evaluated by electron microscopy. Representative TEM images presented in Fig. 2 illustrate the nature of metal dispersion in both supported catalysts. TEM derived histograms given in Fig. 3 demonstrate a narrow size distribution for Ni/Y (number weighted mean Ni diameter = 10 nm) while Co/Y is characterised by a broad distribution of Co particle sizes with a mean size of 25 nm. The unsupported metals are present as large particles in the micron size range, as demonstrated by the SEM images included in Fig. 2. Bulk Ni is characterised by larger agglomerates in the range of 1–5 μm (mean size = 2.5 μm) when compared with Co which exhibited sizes in the range 200–400 nm (mean size = 300 nm).

3.2. Catalytic growth of carbon nanostructures

In the catalytic growth of nanostructured carbon from a hydrocarbon feed, the presence of H_2 in the feed has been proposed to play a beneficial role by initiating hydrocarbon decomposition and exerting additional structural control on the carbon growth [14]. However, when using acetonitrile as the carbon source, H_2 can impede the incorporation of nitrogen into the carbon product, a result that runs counter to the stated objective of this work. At temperatures in excess of 800 °C, acetonitrile decomposes into CN and CH_3 free radicals, which are active fragments for the formation of nitrogen-doped carbon [32]. However, the presence of H_2 in the feed can result in the formation of HCN which is less susceptible to decomposition with a resultant inhibition of carbon growth with an in-built nitrogen component [32]. We have accordingly employed He as the carrier gas in our growth studies. Solid carbon yield (per gram of metal) is plotted as a function of reaction temperature in Fig. 4. Reaction temperature has been reported as a crucial operational variable in catalytic carbon growth [14,16,18]. In the case of the four catalytic systems studied, carbon yield was raised with increasing temperature, achieving the highest values at 1050 °C. There was a detectable decline in yield at higher temperature (1150 °C), a response that has been noted elsewhere in related catalytic systems [16,26,27]. This effect can be attributed to a switch from catalytic to thermal cracking/pyrolysis as a competitive route to carbon production. While appreciable carbon growth was only observed at T > 850 °C over both bulk metals, Ni/Y delivered a measurable carbon yield at 550 °C. Enhanced carbon growth on supported metals has been attributed to metal particle size [15] where smaller supported metal crystallites bear exposed (higher index) planes that favour reactant decomposition. The commonly accepted model for carbon growth from a metal catalyst involves reactant decomposition on the top surface of a metal particle followed by a diffusion of carbon atoms into the metal with precipitation at other facets of the particle [12]. The diffusion coefficient of C in Ni (1.47×10^{-11} m^2 s^{-1} at 950 °C) is higher than that recorded for Co (6.62×10^{-12} m^2 s^{-1} at 950 °C) [33], which would suggest a higher growth rate over Ni. However, in this study, supported Co delivered consistently higher carbon yields (where T > 550 °C) and bulk Co also outperformed Ni (see Fig. 4). It has been proposed that the destructive chemisorption of the hydrocarbon results in the formation of a sub-stoichiometric metal carbide prior to filament formation. It should be noted that formation enthalpies of −9 and −4 kJ mol^{-1} have been recorded for Co_2C and Ni_3C, respectively [34], which indicates that Co carbide formation is thermodynamically more favoured than Ni carbide. It appears that, over our working temperatures, reactant decomposition on the metal surface is the limiting step rather than carbon diffusion rate. Carbon yield as a function of time-on-stream is plotted in Fig. 5 for representative reaction temperatures (750 °C for supported and 950 °C for unsupported systems) that deliver an appreciable carbon deposit. The supported catalysts, Co/Y in particular, show a pronounced initial increase in carbon yield over the

Table 3
BET surface area, porosity, crystalline parameters and elemental (CHN) composition of representative carbon obtained from reaction over bulk and Y zeolite (supported Ni and Co catalysts. Δt = 60 min; 0.73 g_C g_{metal}^{-1} min^{-1}. Carbon obtained in the absence of catalyst is included)

Catalyst/reaction temperature	BET area (m^2 g^{-1})	Ext. surface area (m^2 g^{-1})	Total pore volume (cm^3 g^{-1})	d_{pore} (nm)	d_{002} (nm)	L_c (nm)	Carbon (mol%)	Hydrogen (mol%)	Nitrogen (mol%)
Ni/Y @750 °C	49	36	0.09	7.4	0.343	5.4	90.5	5.0	4.5
Ni/Y@ 950 °C	31	26	0.09	12.1	0.339	6.3	92.6	5.9	1.5
Ni/Y@1150 °C	8	7	0.04	21.1	0.339	5.4	95.2	2.6	2.2
Co/Y@750 °C	100	96	0.33	13.2	0.343	4.7	95.9	2.5	1.6
Co/Y@950 °C	19	12	0.05	12.1	0.339	6.3	95.2	3.6	1.2
Co/Y@1150 °C	5	2	0.02	11.8	0.339	4.7	92.5	4.9	2.6
Ni + Y@950 °C	8	5	0.04	17.5	0.340	6.2	91.1	5.7	3.2
Ni + Y@1150 °C	5	2	0.01	9.2	0.340	3.5	91.7	4.8	3.5
Co + Y@950 °C	5	<1	0.01	8.8	0.343	3.5	89.0	6.0	5.0
Co + Y@1150 °C	5	<1	0.01	9.9	0.338	9.5	90.7	5.7	3.6
None@1150 °C	6	<1	0.01	8.5	0.339	5.0	93.1	2.9	4.0

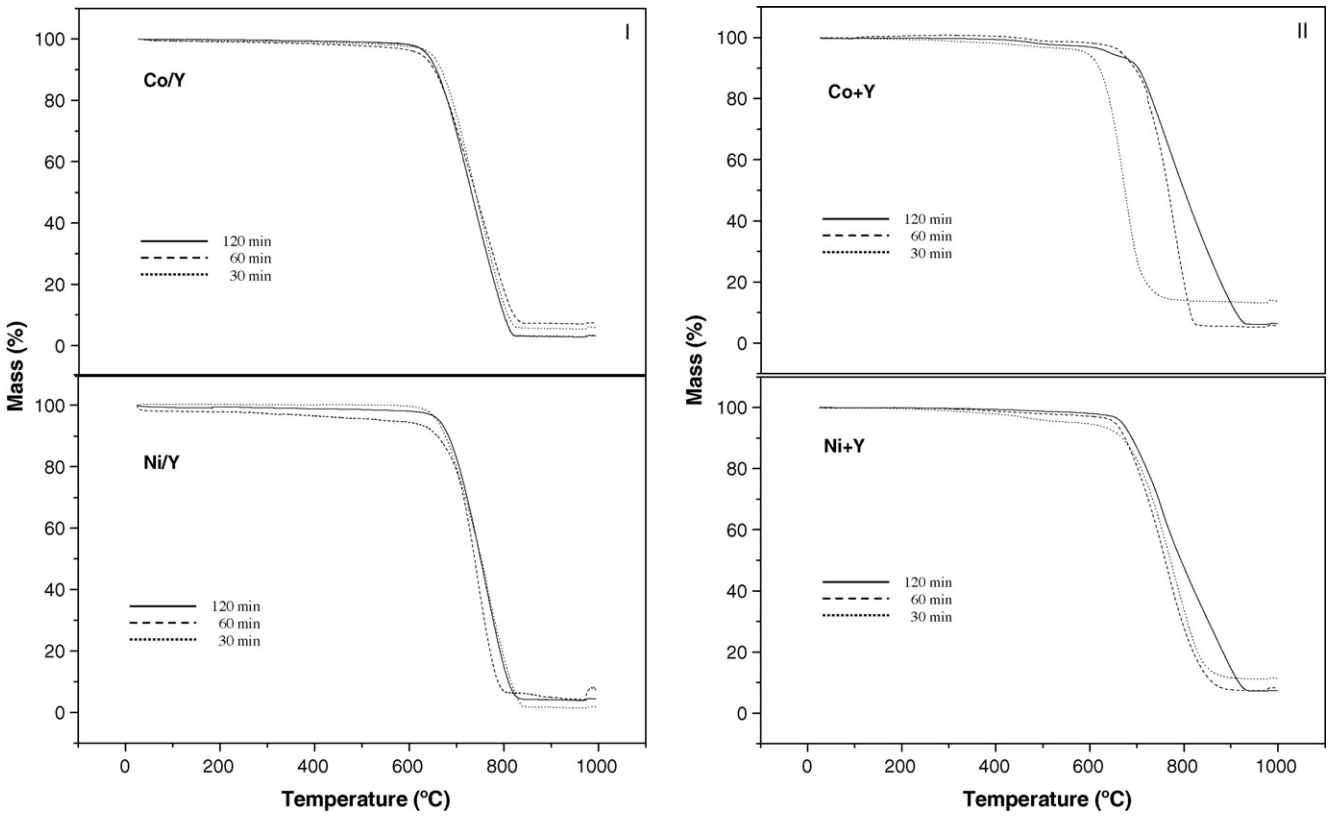

Fig. 7. TPO profiles associated with the carbon obtained after 30 min (dotted line), 60 min (dashed line) and 120 min (solid line) on-stream for reaction over (I) zeolite supported and (II) unsupported Ni and Co catalysts: GHSV = 16,000 h^{-1}; 0.73 $g_C\ g_{metal}^{-1}\ min^{-1}$; T = 750 °C for Ni/Y and Co/Y; T = 950 °C for Ni + Y and Co + Y.

first 0.5 h on-stream followed by a less accused increase in carbon deposition; the less active bulk metals delivered an essentially constant increase in carbon yield during the time interval studied. Loss of activity for supported systems has been reported previously and ascribed to a poisoning of the active metal particle due to encapsulation by carbon [35].

3.3. Carbon characterization

TPO analyses were conducted to probe structural order. It is well established that the more ordered the carbon structure, the higher is the temperature required for gasification during TPO [16]. Representative TPO profiles of carbon samples obtained from reaction over the four catalysts at three synthesis temperatures are presented in Fig. 6. The TPO profiles for carbon deposits obtained at higher reaction temperatures (from 750 to 1150 °C) were consistently shifted to higher gasification temperatures, a response that has been reported elsewhere [35] for carbon growth from a hydrocarbon precursor. As a general observation, carbon grown at higher temperatures gasified over a wider temperature range, suggesting a composite carbon product with a wider range of structural order; this effect is illustrated by the DTG traces included as insets in Fig. 6. TEM results, discussed below, have revealed a structural dependence on growth temperature which can account for the observed TPO response. The ranges of gasification temperatures are recorded in Table 2 and compared with that obtained for a "model"-activated carbon (see Fig. 6III). Based on the TPO results, the catalytically generated carbon is more structured than standard amorphous carbon. The carbon product generated over Ni (bulk and supported) gasified at higher temperatures when compared with that grown over Co (Table 2), what suggests a higher degree of graphitisation. There was no apparent dependency of carbon structural order with time-on-stream (up to 2 h) for reaction over the supported catalysts (see Fig. 7I). However, the TPO of carbon growth on bulk metal (notably Co) exhibited (see Fig. 7II) higher gasification temperatures at longer reaction times. While TPO analysis provides an indirect assessment of carbon structural order, the inferred trends find further support in XRD analyses (see Fig. 8). Each profile exhibits a peak at ca. 25°, i.e., (0 0 2) graphite plane, the broadness of which is indicative of a lesser long range structural order; an ill-defined peak at 43.8° can be assigned to the (1 0 0) graphite plane. We have adopted the interlayer spacing (d_{002}, 0.335 nm for graphite) as a quantitative measure of graphitic character. The d_{002} values recorded in Table 3 are consistent with a graphitic product where the decrease in interlayer spacing with increasing synthesis temperature suggests a better packing of the graphene layers. The crystalline parameter L_c (deduced from the half-width of the (0 0 2) diffraction peak (Table 3)), however, experiences a decrease at the highest temperature, suggestive of a morphological change, as will be commented below.

The nitrogen adsorption–desorption isotherms associated with the carbon deposits (see Fig. 9) exhibit a type IV profile, according to the IUPAC classification. Type IV multilayer adsorption–desorption accompanied by capillary condensation generate hysteresis loops that are diagnostic of mesoporosity; the associated pore sizes presented in Table 2 fall within the accepted mesopore (2–50 nm) range. As a general observation, BET surface area and total pore volume decreased with increasing synthesis temperature. The observed decrease in BET area/pore volume is suggestive of some structural difference. The latter emerges from SEM/TEM analysis; representative SEM/TEM images are presented in Figs. 10–12, wherein a range of carbon structures is in evidence. Acetonitrile decomposition over Ni/Y at 750 °C (Fig. 10a and b) delivered high aspect ratio carbon filaments that exhibited a hollow central core.

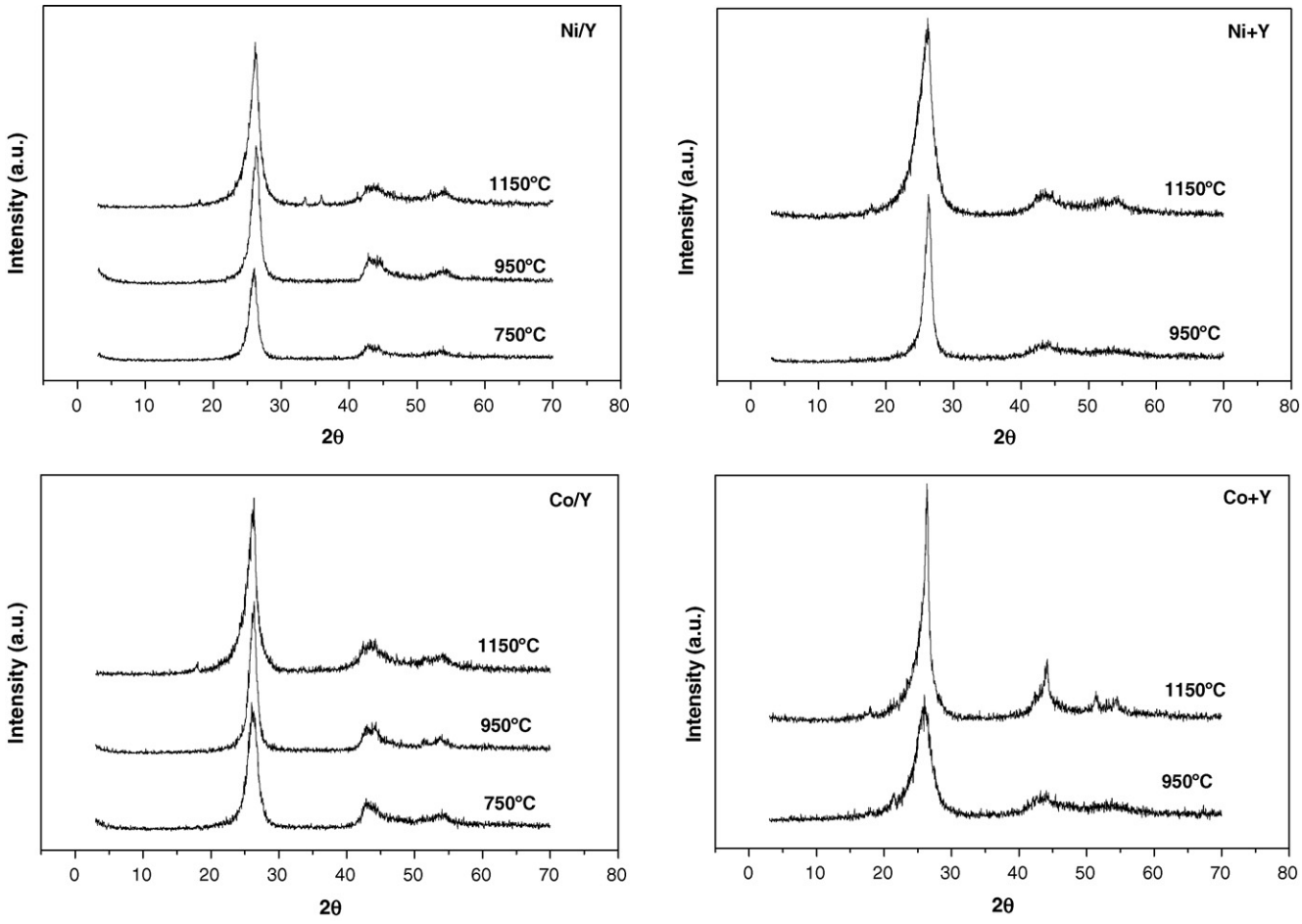

Fig. 8. XRD patterns of the carbon obtained at representative temperatures over the four catalytic systems: GHSV = 16,000 h^{-1}; 0.73 g_C g_{metal}^{-1} min^{-1}; Δt = 60 min.

The occurrence of a hollow core has been attributed to a deformation of the seed metal particle resulting in an unequal diffusion of carbon through the metal particle [16]. The higher resolution image (Fig. 10c) shows graphene layers that are orientated parallel to the growth axis with an interlayer distance of 0.343 nm. Filament diameter varied from 20 to 50 nm, which exceeds the starting Ni particle size diameters in the activated catalyst (see Fig. 3) suggesting a Ni sintering during carbon formation. Acetonitrile decomposition over supported Co (at 750 °C) delivered a similar filamentous growth (Fig. 10d and e), albeit the diameters exhibited a broader size distribution (10–70 nm) than that observed for Ni/Y. Filament size distribution was closer to the starting Co size (see Fig. 3), suggesting that Co did not undergo sintering to the same extent during carbon growth. The high resolution TEM images reveal a series of lattice defects along the length of the filaments generated from Ni/Y (Fig. 10c) and Co/Y (Fig. 10f). This structural response is attributed to differences in bulk and surface C atom diffusion rates that is, in turn, dependent on metal particle shape and size. The images shown in Fig. 10 suggest a pseudo-periodic response, i.e., a periodic fluctuation of carbon concentration.

Reaction at a higher temperature (950 °C) over Ni/Y generated filaments (Fig. 11a and b) with a distinct structure, i.e., no evidence of a central hollow core where the periodicity apparent at the lower temperature is more marked. High resolution micrograph (Fig. 11c) shows how graphene layers lose their alignment parallel to the growth axis to accommodate curved domains. The average interlayer spacing (0.339 nm) is lower than that recorded for the carbon growth at 750 °C (Table 3) and closer to the reference value for graphite. This is in line with the TPO results which suggested enhanced structural order at the higher reaction temperature (see Fig. 6). The filaments produced at the higher temperature exhibited a broader size range (40–200 nm). Carbon filaments grown from bulk Ni (Fig. 11d and e) were even wider and less homogenous in size (100–300 nm) than that obtained from supported Ni. Such a lack of control over the filament diameter has been previously reported in the literature for unsupported systems [12]. Carbon growth from Co/Y at 950 °C also exhibited a wider distribution (70–300 nm) of larger diameters when compared with the lower temperature growth. Moreover, the arrangement of graphene sheets exhibits significant lattice structural disruption (Fig. 11g and h). The high resolution micrograph (Fig. 11i) reveals, as in the case of Ni/Y, a periodic curvature. Periodicity in filament growth has been attributed in literature [36] to a pulsating growth that is related to the thermodynamic stability of the metal carbide. The carbon generated from Co + Y at 950 °C was not in the form of filaments but rather as a clustering of spheres (Fig. 11j and k) with diameters in the range 100–150 nm. The high resolution TEM image (Fig. 11l) illustrates how the graphene sheets accommodate the curvature of the sphere with an interlayer lattice spacing of 0.343 nm. When the temperature was raised to 1150 °C, Ni/Y also delivered a spherical product as shown in Fig. 12a–c. The spheres are not present as discrete entities but rather a conglomeration or clustering of the spheres is in evidence with diameters in the range of 150–200 nm. An essentially equivalent pseudo-spheroidal structure with a similar size range (150–200 nm) was also generated at the same temperature using unsupported Ni (see Fig. 12d–f) which

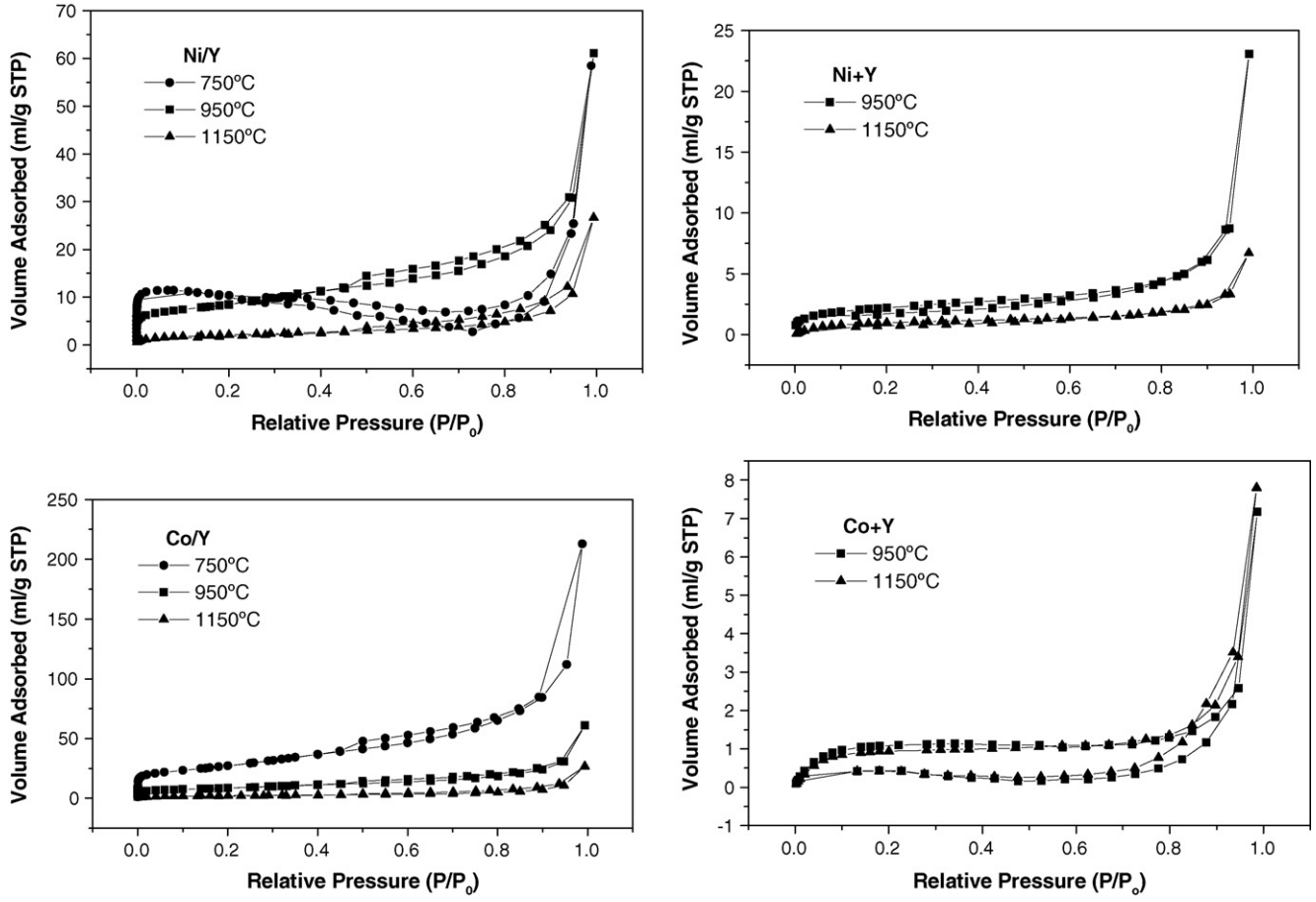

Fig. 9. N_2 adsorption–desorption isotherms associated with the carbon obtained at representative temperatures over the four catalytic systems: GHSV = 16,000 h^{-1}; 0.73 g_C $g_{metal}{}^{-1}$ min^{-1}; Δt = 60 min.

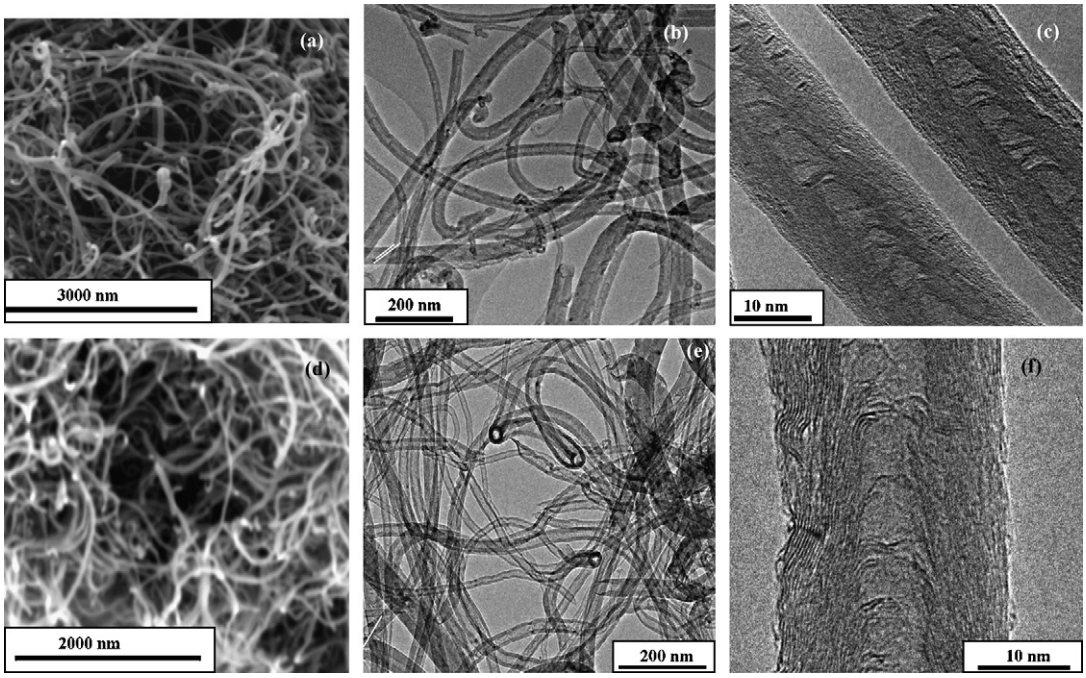

Fig. 10. Representative micrographs of the carbon obtained over Ni/Y (a: SEM low magnification image; b: TEM low magnification image; c: TEM high magnification image) and Co/Y (d: SEM low magnification image; e: TEM low magnification image; f: TEM high magnification image) for reaction at 750 °C: GHSV = 16,000 h^{-1}, 0.73 g_C $g_{metal}{}^{-1}$ min^{-1}, Δt = 60 min.

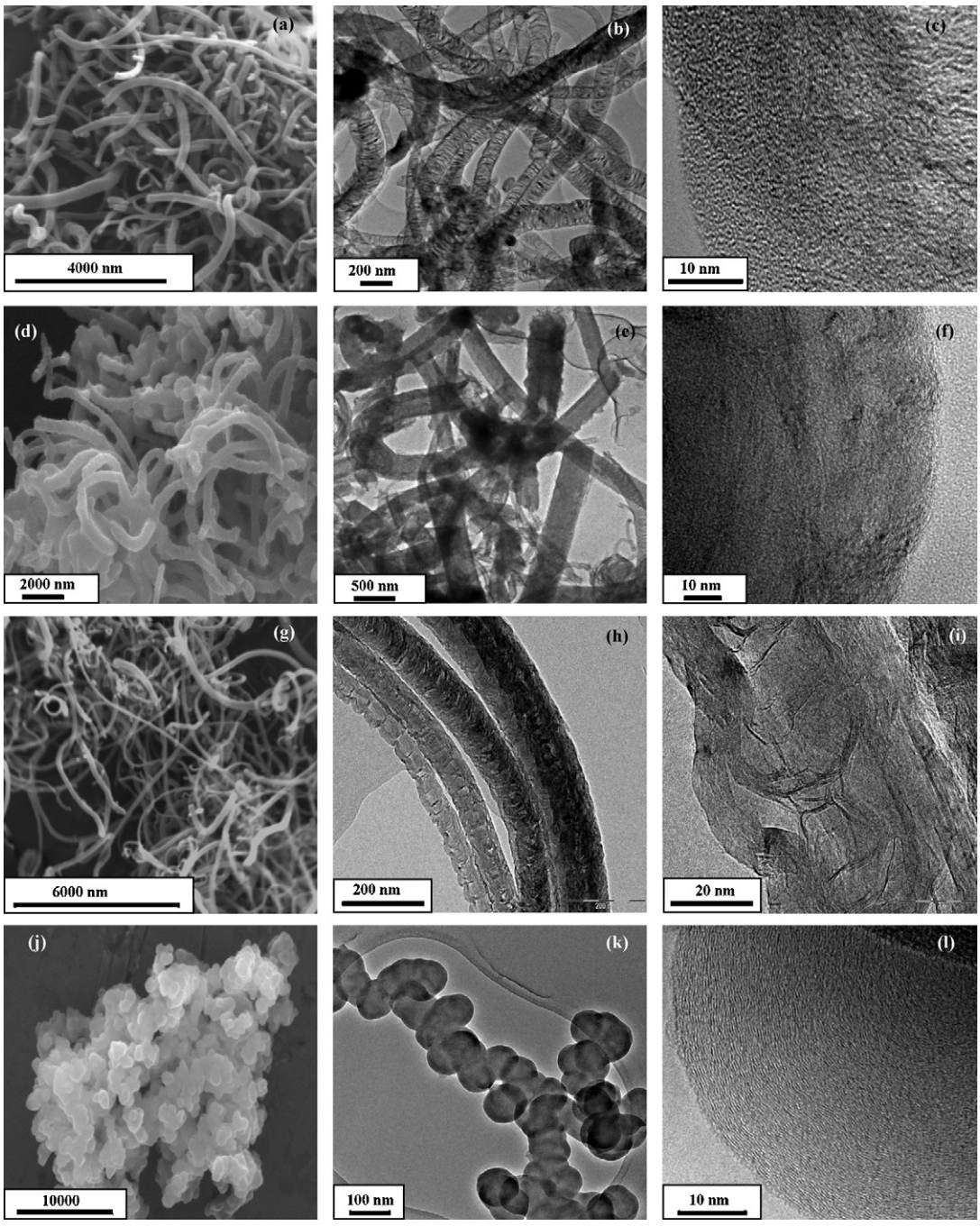

Fig. 11. Representative micrographs of the carbon obtained over Ni/Y (a: SEM low magnification image; b: TEM low magnification image; c: TEM high magnification image), Ni + Y (d: SEM low magnification image; e: TEM low magnification image; f: TEM high magnification image), Co/Y (g: SEM low magnification image; h: TEM low magnification image; i: TEM high magnification image) and Co + Y (j: SEM low magnification image; k: TEM low magnification image; l: TEM high magnification image) for reaction at 950 °C: GHSV = 16,000 h^{-1}, 0.73 $g_C\ g_{metal}^{-1}\ min^{-1}$, Δt = 60 min.

suggests that, at this temperature, the support has little effect on the carbon product size and/or structure. In contrast, under the same growth conditions Co/Y produced a combination of filamentous carbon and spheres (Fig. 12g–i). Bulk Co generated spherical carbon as the predominant product (see Fig. 12j–l). The low BET area associated with those carbons obtained at the higher reaction temperatures (see Table 3) can be attributed to the predominant spherical morphology: the sphere as a geometrical body presents the lowest exposed specific surface area. Carbon nanospheres have been reported to possess limited porosity [37], which is in line with the results presented in Table 3. The trends observed in this study in terms of the dependence of carbon structure and dimensions on catalyst and reaction temperature are summarised in Table 4.

The production of carbon nanospheres is gaining increasing interest due to novel applications of these materials in fuel cells, secondary Li ion batteries, as lubricants or polymer additives [38,39]. Carbon nanosphere production has been reported via mixed-valent oxide decomposition of natural gas at 1100 °C [40] and the decomposition of pentane over $Fe(CO)_5$ at temperatures in excess of 900 °C [41]. However, thermal pyrolysis has been successfully employed to generate nanospheres from a diverse feedstock (methane, benzene, styrene, mesitylene, etc.) at temperatures

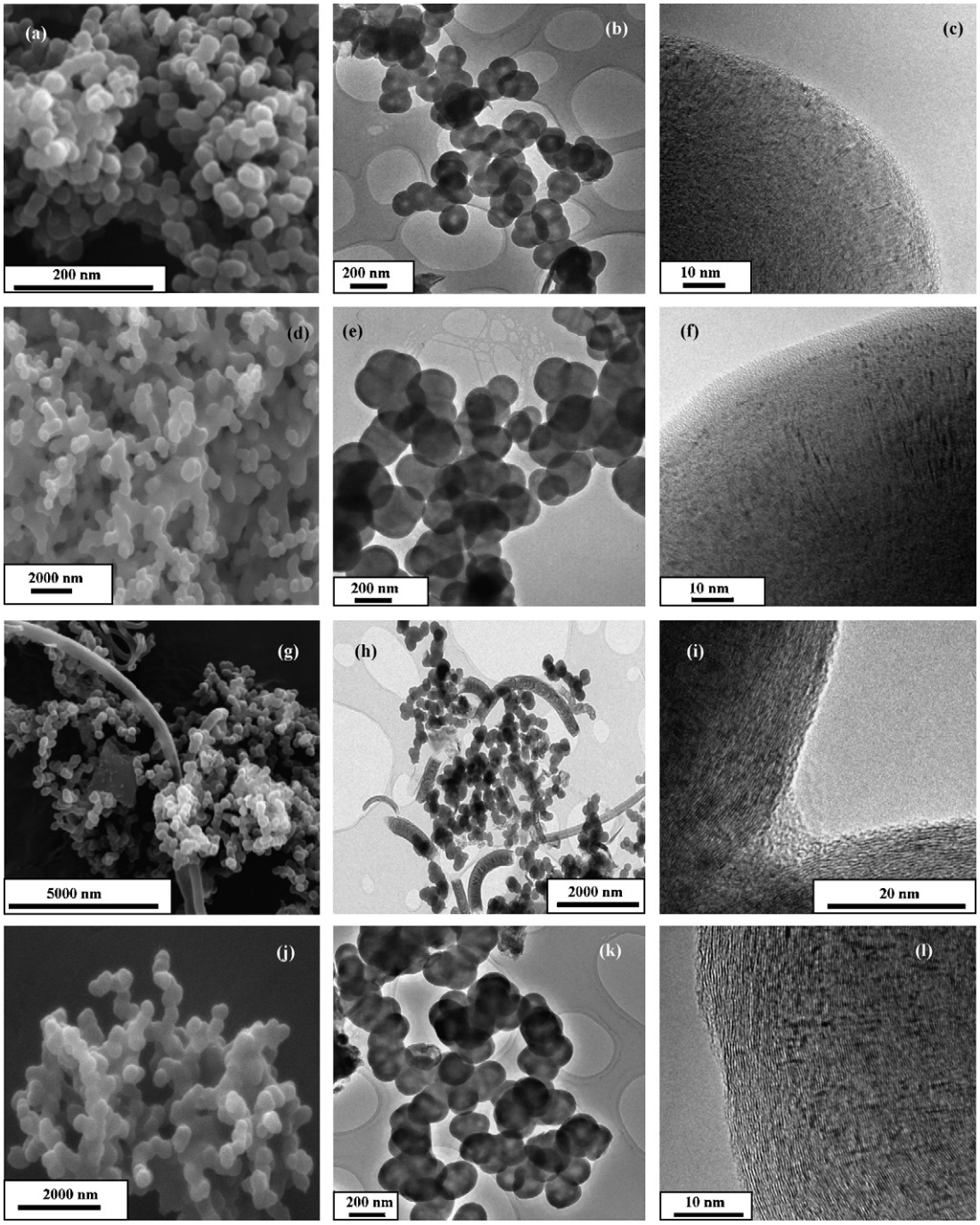

Fig. 12. Representative micrographs of the carbon obtained over Ni/Y (a: SEM low magnification image; b: TEM low magnification image; c: TEM high magnification image), Ni + Y (d: SEM low magnification image; e: TEM low magnification image; f: TEM high magnification image), Co/Y (g: SEM low magnification image; h: TEM low magnification image; i: TEM high magnification image) and Co + Y (j: SEM low magnification image; k: TEM low magnification image; l: TEM high magnification image) for reaction at 1150 °C: GHSV = 16,000 h^{-1}, 0.73 $g_C\ g_{metal}^{-1}\ min^{-1}$, Δt = 60 min.

greater than 1000 °C [39]. Consequently, runs at the highest temperatures (at which the spheres were obtained) were performed in the absence of a catalyst (Tables 2–4) delivering essentially similar results both in yield and structure/morphology than when a catalyst was used. One the one hand, this result supports the carbon production drop occurred at 1150 °C, temperature at which thermal pyrolysis is responsible for carbon growth, rather than the catalytic route, also in line with the essentially coincident yields obtained independently of the catalyst employed. On the other hand, carbon morphology was predominantly the same for the four catalysts (regarded the presence of filaments in the case of the most active Co/Y, diagnostic of residual catalytic activity). The spherical morphology has been reported in literature to posses a lower crystalline character than filaments [35], due to imperfections and reactive dangling bonds present in their surface. In this line, the average interlayer spacing d_{002}, that did not show appreciable differences between spheres and those filaments obtained at high temperatures find further support in the average crystalline parameter, L_c, which experienced a decrease when the carbonaceous product switched from filaments to spheres (Table 3). Regarding the TPO

Table 4
Nature of the predominant carbon growth and diameter range generated for reaction over the four catalyst systems at representative reaction temperatures: $\Delta t = 60$ min; 0.73 $g_C\ g_{metal}^{-1}\ min^{-1}$ (carbon obtained in the absence of catalyst is included)

Catalyst	Temperature (°C)	Predominant carbon structure	Size range (nm)
Ni/Y	750	Filaments	20–50
Ni/Y	950	Filaments	40–200
Ni/Y	1150	Spheres	150–200
Ni + Y	950	Filaments	100–300
Ni + Y	1150	Spheres	150–200
Co/Y	750	Filaments	10–70
Co/Y	950	Filaments	70–300
Co/Y	1150	Filaments + Spheres	100–200
Co + Y	950	Spheres	100–150
Co + Y	1150	Spheres	100–200
None	1150	Spheres	100–200

response, higher gasification temperatures associated to spheres is tentatively attributed to a further graphitization/reduction of amorphous carbon formed rather than an increase in the crystalline character. In previous work [13] we established that high aspect ratio carbon nanofilaments were the sole structured carbon product generated from the decomposition of ethylene over Ni loaded zeolites. A switch from a predominantly filamentous to a spherical product necessitates a quite distinct growth mechanism, where thermal decomposition seems in the present work to conduct the process, rather than the catalytic route. It is worth flagging the work of Inagaki, who developed a comprehensive study on the growth mechanism of spherical carbon, where small domains of graphitic hexagonal layers of carbon atoms, known as basic structural units (BSUs) are arranged to form the final spherical shape [42]. In this line, there is some agreement in literature that not only hexagonal layers, but also pentagonal and heptagonal ones are needed to accommodate the curvature of the sphere [40].

Nitrogen incorporation was investigated by means of elemental (CHN) analysis which demonstrated (see Table 3) a bulk nitrogen content up to 5 mol%, which is comparable with values reported in literature. Trasobares and co-workers reported nitrogen contents of 3–5 mol% from the pyrolysis (550–1000 °C) of melamine over Ni and Fe powders [43]. Tang et al. obtained a nitrogen content of 2–16 mol% from the decomposition (650–1175 °C) of dimethylformamide over Fe/Al_2O_3 [23] while Lee et al. reported 2–6 mol% nitrogen after the decomposition (900–1100 °C) of CH_4/NH_3 and C_2H_2/NH_3 over Fe/Si [44]. Nakajima and Koh [45] reported an optimum temperature range between 850 and 1000 °C for nitrogen incorporation in carbon generated from the decomposition of acetonitrile and pyridine. Kudashov et al. [46] noted that the reaction of acetonitrile over Co resulted in a lesser nitrogen incorporation in the nanotubes formed than that recorded for Ni, a response that is not obvious from our measurements. It is well documented that the incorporation of heteroatoms into structured carbon, even at a low mass/mole percent, can induce lattice defects in the graphene layers [46]. This effect can account, at least in part for the disruption to the carbon lattice structure that is illustrated by the TEM images presented in Figs. 10 and 11, as by the crystalline parameter L_c, which decreased with increasing nitrogen content (Table 3).

4. Conclusions

Chemical vapour decomposition (CVD) of acetonitrile over both Y zeolite supported and unsupported Ni and Co catalysts has been shown as an effective route for the production (up to 35 g_{carbon}/g_{metal}) of ordered carbonaceous materials with a significant (up to 5 mol%) nitrogen content. The supported systems generated significantly higher carbon yields where carbon growth was initiated at temperatures up to 300 °C lower than that required for measurable carbon growth from the bulk metals. Under conditions of maximum carbon growth, bulk and Y zeolite supported Co delivered higher specific carbon yields than Ni, a response that we tentatively attribute to enhanced reactant decomposition/carbide formation associated with Co. An increase in reaction temperature (up to 1050 °C) was accompanied by an elevation of carbon yield and an accompanying increase in structural order, based on TPO analyses. Gasification temperatures derived from TPO analyses suggest that the carbon produced by the Ni catalysts is more ordered. XRD analyses were, in all the cases, consistent with a graphitic product. On the basis of the TPO measurements, time-on-stream variations had no significant effect on carbon structure for growth over the supported metals but there is evidence of a temporal enhancement in the case of the bulk (particulary Co) metals. A slight loss of activity with time-on-stream was a feature of reaction over the supported metals and can be attributed to poisoning (metal encapsulation) by the greater quantities of carbon produced. Carbon produced at lower reaction temperatures took the form of high aspect ratio filamentous structures with an inter-platelet spacing of ca. 0.34 nm and a hollow central core. The filament diameters exceeded the starting metal (notably Ni) particle size, suggesting a reaction induced metal sintering. An increase in reaction temperature resulted in a disruption to the lattice structure with, at the highest temperature studied (1150 °C), the formation of carbon nanospheres as the predominant carbon morphology. Nanosphere formation was investigated in the absence of a catalyst, concluding that its formation is rather attributable to thermal pyrolysis than to a catalytic route. The presence of nitrogen in the carbon structures was closely linked to carbon morphology, being favoured in those structures presenting a higher degree of structural defects. However, there is no clear correlation between the catalyst used and the degree of nitrogen inclusion in the carbon product. Taking an overview of the results presented, the catalytic decomposition of acetonitrile is an effective route for the production of nitrogen-doped nanostructured carbon where variations in the nature of the catalytic metal and reaction temperature can be used to control the structure/morphology of the carbon product.

Acknowledgments

The authors acknowledge financial support from Consejería de Ciencia y Tecnología de la Junta de Comunidades de Castilla-La Mancha (Project PBI-05-038 and PCI08-0020). Agustín Garrido and Prof. Mark A. Keane are gratefully acknowledged for helpful discussions.

References

[1] S. Ijima, Helical microtubules of graphitic carbon, Nature 354 (1991) 56–58.
[2] C. Park, E.S. Ángel, A. Crowe, T.R. Gilbert, N.M. Rodríguez, Use of carbon nanofibers in the removal of organic solvents from water, Langmuir 16 (2000) 8050–8056.
[3] Y. Fan, B. Liao, M. Liu, Y. Yei, M. Lu, H. Cheng, Hydrogen uptake in vapor-grown carbon nanofibers, Carbon 37 (1999) 1649–1652.
[4] C.N.R. Rao, Novel materials, materials design and synthetic strategies: recent advances and new directions, J. Mater. Chem. 9 (1999) 1–14.
[5] H. Markus, A.J. Plomp, T. Sandberg, V. Nieminen, J.H. Bitter, D.Y. Murzin, Dehydrogenation of hydroxymatairenisol to oxomatairenisol over carbon nanofibre-supported palladium catalysts, J. Mol. Catal. A: Chem. 274 (2007) 42–49.
[6] C. Wang, M. Waje, X. Wang, J.M. Tang, R.C. Haddon, Y.S. Yan, Proton exchange membrane fuel cells with carbon nanotube based electrodes, Nano Lett. 4 (2004) 345–348.
[7] O. Stephan, P.M. Ajayan, C. Colliex, Ph. Redlich, J.M. Lambert, P. Bernier, P. Lefin, Doping graphitic and carbon nanotube structures with boron and nitrogen, Science 266 (1994) 1683–1685.

[8] M. Glerup, M. Castignoles, M. Holzinger, G. Hug, A. Loiseau, P. Bernier, Synthesis of highly nitrogen-doped multi-walled carbon nanotubes, Chem. Commun. (2003) 2542–2543.
[9] T. Maiyalagan, B. Viswanathan, Template synthesis and characterization of well-aligned nitrogen containing carbon nanotubes, Mater. Chem. Phys. 93 (2005) 291–295.
[10] M. Glerup, J. Steinmetz, D. Samaille, O. Stephan, S. Enouz, A. Loiseau, S. Roth, P. Bernier, Synthesis of N-doped SWNT using the arc-discharge procedure, Chem. Phys. Lett. 387 (2004) 193–197.
[11] Y. Zhang, H. Gu, K. Suenaga, S. Iijima, Heterogeneous growth of B-C-N nanotubes by laser ablation, Chem. Phys. Lett. 279 (1997) 264–269.
[12] K.P. de Jong, J.W. Geus, Carbon nanofibers: catalytic synthesis and applications, Catal. Rev. Sci. Eng. 42 (2000) 481–510.
[13] A. Romero, A. Garrido, A. Nieto-Márquez, P. Sánchez, A. de Lucas, J.L. Valverde, Synthesis and structural characteristics of highly graphitized carbón nanofibers produced from the catalytic decomposition of ethylene: Influence of the active metal (Co, Ni, Fe) and the zeolite type support, Micropor. Mesopor. Matter 110 (2008) 318–329.
[14] C. Park, N.M. Rodriguez, R.T.K. Baker, Carbon deposition on iron–nickel during interaction with carbon monoxide–hydrogen mixtures, J. Catal. 169 (1997) 212–227.
[15] M.L. Toebes, J.H. Bitter, A.J. van Dillen, K.P. de Jong, Impact of the structure and reactivity of nickel particles on the catalytic growth of carbon nanofibers, Catal. Today 76 (2002) 33–42.
[16] C. Park, M.A. Keane, Catalyst support effects in the growth of structured carbon from the decomposition of ethylene over nickel, J. Catal. 221 (2004) 386–399.
[17] C.J. Lee, J. Park, Y. Huh, J.Y. Lee, Temperature effect on the growth of carbon nanotubes using thermal chemical vapor deposition, Chem. Phys. Lett. 343 (2001) 33–38.
[18] K. Hernadi, A. Fonseca, J.B. Nagy, D. Bernaerts, A. Fudala, A.A. Lucas, Catalytic synthesis of carbon nanotubes using zeolite support, Zeolites 17 (1996) 416–423.
[19] Z. Yu, D. Chen, B. Tøtdal, A. Colmen, Effect of support and reactant on the yield and structure of carbon growth by chemical vapour deposition, J. Phys. Chem. B 109 (2005) 6096–6102.
[20] C. Park, R.T.K. Baker, Carbon deposition on iron–nickel during interaction with ethylene–hydrogen mixtures, J. Catal. 179 (1998) 361–374.
[21] M.A. Ermakova, D.Y. Ermakov, G.G. Kuvshinov, L.M. Plyasova, New nickel catalysts for the formation of filamentous carbon in the reaction of methane decomposition, J. Catal. 187 (1999) 77–84.
[22] R. Sen, B.C. Satishkumar, A. Govindaraj, K.R. Harikumar, M.K. Renganathan, C.N.R. Rao, Nitrogen-containing carbon nanotubes, J. Mater. Chem. 7 (1997) 2335–2337.
[23] C. Tang, Y. Bando, D. Golberg, F. Xu, Structure and nitrogen incorporation of carbon nanotubes synthesized by catalytic pyrolysis of dimethylformamide, Carbon 42 (2004) 2625–2640.
[24] F. Kapteijn, J.A. Moulijn, S. Matzner, H.P. Boehm, The development of nitrogen functionality in model chars during gasification in CO_2 and O_2, Carbon 37 (1999) 1143–1150.
[25] M. Glerup, M. Castignolles, M. Holzinger, H. Kanzow, A. Loiseau, P. Bernier, Synthesis of C and CN_x nanotubes, using the aerosol method, Mater. Res. Soc. Symp. Proc. 772 (2003) 99.
[26] A. de Lucas, A. Garrido, P. Sánchez, A. Romero, J.L. Valverde, Growth of carbon nanofibers from Ni/Y zeolite based catalysts: effects of Ni introduction method, reaction temperature and reaction gas composition, Ind. Eng. Chem. Res. 44 (2005) 8225–8263.
[27] A. de Lucas, P.B. García, A. Garrido, A. Romero, J.L. Valverde, Catalytic synthesis of carbon nanofibers with different graphene plane alignments using Ni deposited on iron pillared clays, Appl. Catal. A: Gen. 301 (2006) 123–132.
[28] K.V. Murthy, P.M. Patterson, M.A. Keane, C–X bond reactivity in the catalytic hydrodehalogenation of haloharenes over unsupported and silica supported Ni, J. Mol. Catal. A: Chem. 225 (2005) 149–160.
[29] P. Arnoldy, J.A. Moulijn, Temperature-programmed reduction of CoO/Al_2O_3 catalysts, J. Catal. 93 (1985) 38–54.
[30] R. Nares, J. Ramírez, A. Gutiérrez-Alejandre, C. Louis, T. Klimova, Ni/Hβ-zeolite catalysts prepared by deposition–precipitation, J. Phys. Chem. B 106 (2002) 13287–13293.
[31] B. Pawelec, P. Castaño, J.M. Arandes, J. Bilbao, S. Thomas, M.A. Peña, J.L.G. Fierro, Factors influencing the thioresistance of nickel catalysts in aromatics hydrogenation, Appl. Catal. A: Gen. 317 (2007) 20–33.
[32] Y. Hao, L. Qingwen, Z. Jin, L. Zhongfan, The effect of hydrogen on the formation of nitrogen-doped carbon nanotubes via catalytic pyrolysis of acetonitrile, Chem. Phys. Lett. 380 (2003) 347–351.
[33] H. Yokohama, H. Numakura, M. Koiwa, The solubility and diffusion of carbon in palladium, Acta Mater. 46 (1998) 2823–2830.
[34] A.K. Niessen, F.R. de Boer, R. Boom, P.F. de Chatel, W.C.M. Mattens, Model predictions for the enthalpy of formation of transition alloys II, CALPHAD 7 (1983) 51–70.
[35] A. Nieto-Márquez, J.L. Valverde, M.A. Keane, Catalytic growth of structured carbon from chloro-hydrocarbons, Appl. Catal. A: Gen. 332 (2007) 237–246.
[36] S. van Dommele, A. Romero-Izquirdo, R. Brydson, K.P. de Jong, J.H. Bitter, Tuning nitrogen functionalities in catalytically grown nitrogen-containing carbon nanotubes, Carbon 46 (2008) 138–148.
[37] Ph. Serp, R. Feurer, P. Kalck, Y. Kihn, J.L. Faria, J.L. Figueiredo, A chemical vapour deposition process for the production of carbon nanospheres, Carbon 39 (2001) 621–626.
[38] P. Serp, R. Feurer, Y. Kihn, J.L. Faria, J.L. Figueiredo, Novel carbon supported material: highly dispersed platinum particles on carbon nanospheres, J. Mater. Chem. 11 (2001) 1980–1981.
[39] H.-S. Qian, F.-M. Han, B. Zhang, Y.-C. Guo, J. Yue, B.-X. Peng, Non-catalytic CVD preparation of carbon spheres with a specific size, Carbon 42 (2004) 761–766.
[40] Z.L. Wang, K.C. Kang, On accretion of nanosize carbon spheres, J. Phys. Chem. 100 (1996) 5163–5165.
[41] X.-Y. Liu, B.-C. Huang, N.J. Coville, The $Fe(CO)_5$ catalyzed pyrolysis of pentane: carbon nanotube and carbon nanoball formation, Carbon 40 (2002) 2791–2799.
[42] M. Inagaki, Carbon materials: structure, texture and intercalation, Solid State Ionics 86–88 (1996) 833–839.
[43] S. Trasobares, O. Stephan, C. Colliex, W.K. Hsu, H.W. Kroto, D.R.M. Walton, Compartmentalized CN_x nanotubes: chemistry, morphology, and growth, J. Chem. Phys. 116 (2002) 8966–8972.
[44] Y.T. Lee, N.S. Kim, S.Y. Bae, J. Park, S.-C. Yu, H. Ryu, H.J. Lee, Growth of vertically aligned nitrogen-doped carbon nanotubes: control of the nitrogen content over the temperature range 900–1100 °C, J. Phys. Chem. B 107 (2003) 12958–12963.
[45] T. Nakajima, M. Koh, Synthesis of high crystalline carbon–nitrogen layered compounds by CVD using nickel and cobalt catalysts, Carbon 35 (1997) 203–208.
[46] A.G. Kudashov, A.V. Okotrub, L.G. Bulusheva, I.P. Asanov, Y.V. Shubin, N.F. Yudanov, L.I. Yudanova, V.S. Danilovich, O.G. Abrosinov, Influence of Ni–Co catalyst composition on nitrogen content in carbon nanotubes, J. Phys. Chem. B 108 (2004) 9048–9053.